ORGANIC CHEMISTRY FRONTIERS

RESEARCH ARTICLE

View Article Online
View Journal | View Issue

Cite this: *Org. Chem. Front.*, 2026, **13**, 1014

Class-II-aldolase-mimicking polyfunctional Lewis acid/azolium–aryloxide catalysts in direct enantioselective nitro-aldol additions

Khushbu Jangid,†[a] Lisa A. Schmoltzi, †[b] Alexander Allgaier,[c] Radhika Kataria,[c] Daniel M. Wanner,[a] Justin Herrmann,[a] Janis Gschwind,[a] Silvio Münch,[c] Joris van Slageren, [c] Johannes Kästner [b] and René Peters *[a]

The catalytic asymmetric nitroaldol reaction is a powerful tool for accessing chiral 1,2-difunctionalized motifs, and numerous catalytic systems have been reported. Despite considerable progress in achieving high levels of stereocontrol, key challenges persist. In particular, optimal selectivity often requires cryogenic conditions, resulting in prolonged reaction times and limited practicality. In this article, a novel concept for asymmetric nitroaldol additions is introduced through a polyfunctional catalyst. This system integrates a Lewis acid, Co(II), with an azolium–aryloxide betaine, and exhibits mechanistic features reminiscent of class-II aldolases. The proposed mode of action is supported by comprehensive DFT calculations, microkinetic simulations, and detailed spectroscopic analyses. By the unique synergistic interplay of the Lewis acidic metal center, the aryloxide as Brønsted base and the corresponding aromatic alcohol serving as both hydrogen bond donor and Brønsted acid, high stereoselectivity was accomplished even at slightly elevated temperature for $MeNO_2$. Like in class-II-aldolases, the aldehyde is activated by H-bonding to the aromatic alcohol and not by the Lewis acid. The latter serves to stabilize and direct the nitronate. The computational studies further demonstrate that the catalyst's key functional groups precisely orchestrate all accompanying transformations. As a result of the mild reaction conditions, not necessitating the use of an external base, the method also proved to be applicable to readily enolizable aliphatic aldehydes, such as phenylacetaldehyde.

Received 12th November 2025,
Accepted 16th December 2025

DOI: 10.1039/d5qo01558h

rsc.li/frontiers-organic

Introduction

The catalytic nitroaldol- or Henry-reaction is a well-established way for forming C,C bonds between nitroalkanes and aldehydes or ketones.[1] The resulting β-nitroalcohols are versatile intermediates that can undergo a wide range of synthetically valuable transformations. These include for instance dehydrations to form conjugated nitroalkenes,[2] reductions to β-amino alcohols,[3] denitrations,[3] oxidation reactions to α-nitroketones[4] and Nef reactions to give α-hydroxy carbonyl derivatives.[5]

Highly enantioenriched β-nitroalcohols have been widely employed in the synthesis of key intermediates for accessing biologically active compounds, including natural products, insecticides, fungicides, and antibiotics.[6–15] Moreover, highly enantioenriched β-amino alcohols, resulting from reduction of the nitro group, are found in numerous active pharmaceutical ingredients,[16–30] underscoring the importance of the nitroaldol reaction as a valuable source of chiral building blocks.[3]

Since the first reports of an asymmetric version of this reaction using chiral lanthanum and heterobimetallic lanthanum/lithium complexes,[31–35] the development of efficient catalytic systems and the synthetic applications of nitroaldol products have attracted substantial attention.[8,36] Different synthetic challenges were addressed through the design of various catalyst types. In particular, chiral Lewis acid catalysts based on copper,[37–58] zinc,[59–64] chromium,[65–68]cobalt[69–74] and rare-earth metal centers[75–79] making use of ligands such as amino acids,[80] amino alcohols,[81–88] oxazolines,[89–95] diamines,[96,97] Schiff bases[98,99]and salen ligands[60,100–103] were reported. Additionally, a range of chiral organocatalyst types such as guanidines, thioureas, cinchona alkaloid derivatives and quaternary ammonium salts have proven effective for enantioselective methods.[36,104,105]

[a]*Universität Stuttgart, Institut für Organische Chemie, Pfaffenwaldring 55, D-70569 Stuttgart, Germany. E-mail: rene.peters@oc.uni-stuttgart.de*
[b]*Universität Stuttgart, Institut für Theoretische Chemie, Pfaffenwaldring 55, D-70569 Stuttgart, Germany*
[c]*Universität Stuttgart, Institut für Physikalische Chemie, Pfaffenwaldring 55, D-70569 Stuttgart, Germany*
† Both authors contributed equally.

The first reported cobalt-catalyzed asymmetric nitroaldol reactions were developed by Yamada *et al.* using salen complexes in combination with an external base.[73] Following this, several other research groups reported highly enantioselective cobalt–salen catalysts.[67,70–72]

These methods typically required extended reaction times and cryogenic temperatures for satisfactory yields and high enantioselectivity. Although other cobalt-based catalysts, such as BOX[69]and amino acid complexes,[74] have been reported, their catalytic performance has generally been inferior.

Here, we report a different concept making use of a new polyfunctional Co(II)-/1,2,3-triazolium–aryloxide catalyst system combining Lewis acid, Brønsted base and hydrogen-bonding activation. Very detailed DFT studies show that the Co(II) center does not activate the aldehyde, but stabilizes the nitronate, which is formed by deprotonation of the nitroalkane by the catalyst's Co-naphthoxide moiety. The thus formed naphthol OH group then activates the aldehyde by hydrogen bonding[106] in close proximity to the Co-nitronate, resulting in a quasi intramolecular C,C-bond forming transition state. The naphthol finally delivers the proton to the alcoholate intermediate formed during the 1,2-addition step (Scheme 1, bottom).

The polyfunctional catalyst thus promotes each individual step of this reaction, avoiding the need for an external base. The mode of action is highly reminiscent of class-II aldolases, which operate in an analogous way: the combination of a Lewis acid (including Co(II))[107] and a Brønsted base (typically glutamate) enable the formation of a metal-stabilized enolate. Meanwhile a tyrosine's aromatic alcohol function is typically responsible for simultaneous activation of the aldehyde substrate by hydrogen bonding and protonation of the alcoholate generated during the C,C-bond forming step (Scheme 1, bottom).[107] Using a class-II-aldolase-mimicking approach, the title reaction proceeds efficiently without the need for low temperatures using nitromethane.

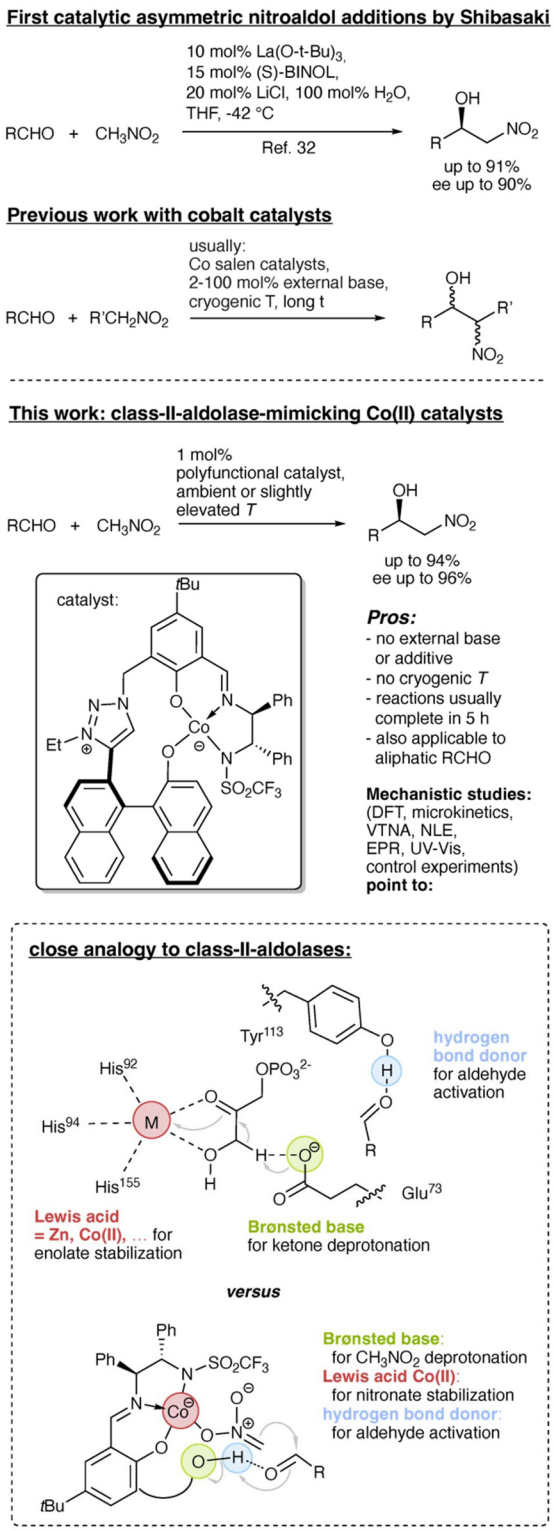

Scheme 1 Top: Pioneering work of the asymmetric nitroaldol addition by Shibasaki and previous work on Co-catalysis. Bottom: direct aldol additions by the new polyfunctional Co(II)-/azolium–aryloxide catalyst and its activation analogy to class-II-aldolases.

Results and discussion

Development of the method

The investigation began with our previously reported Cu(II)/imidazolium–naphthoxide catalyst **C1** (Table 1),[108–112] choosing the 1,2-addition of nitromethane to 2-naphthylcarbaldehyde (**1a**) as model reaction. With 5 mol% **C1** in THF at 25 °C for 20 h, nearly racemic product **2a** was formed in small quantities (9%, entry 1). Changing to the corresponding Co(II) catalyst **C2**,[113] the product yield was significantly increased, while enantioselectivity was still poor (entry 2). Our previously reported Cu(II) and Ni(II)/1,2,3-triazolium–naphthoxide catalysts **C3** (entry 3)[114] and **C4**[113] (entry 4) performed on a similar level. The related new Co(II) catalyst **C5** also featuring a 1,2,3-triazolium unit allowed for improved productivity (60% yield, entry 5), while its diastereomer **C6**, differing in the configuration of the iminosulfonamide ligand motif, provided slightly inferior results (entry 6). Note that all yields reported in

Table 1 Development of the enantioselective addition of nitromethane to the model aldehyde using polyfunctional Lewis acid/azolium–aryloxide catalysts

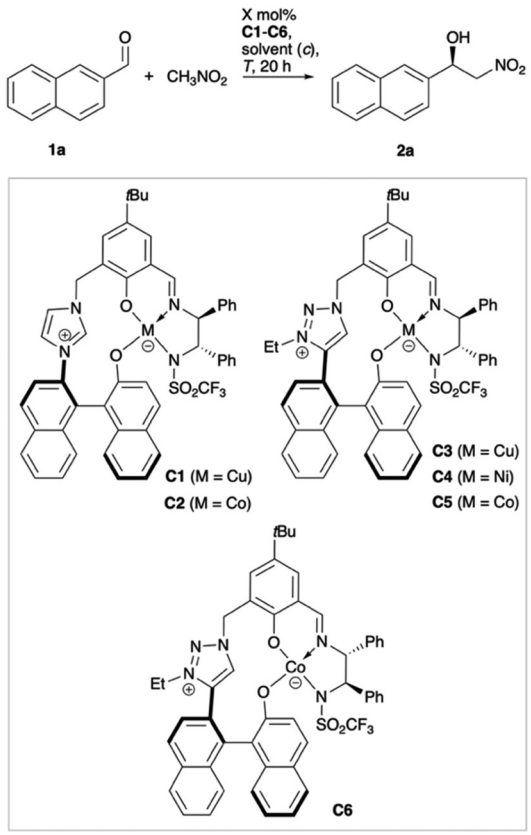

#	C	X (mol%)	Solvent (c/mol L^{-1})	T/°C	Yield[a]/%	ee[b]/%
1	**C1**	5	THF (0.2)	25	09	11
2	**C2**	5	THF (0.2)	25	41	19
3	**C3**	5	THF (0.2)	25	15	19
4	**C4**	5	THF (0.2)	25	22	14
5	**C5**	5	THF (0.2)	25	60	20
6	**C6**	5	THF (0.2)	25	49	15
7	**C5**	5	THF (1.0)	25	80	91
8	**C5**	5	Toluene (1.0)	25	66	60
9	**C5**	5	MeCN (1.0)	25	43	69
10	**C5**	5	DCM (1.0)	25	25	55
11	**C5**	5	CH_3NO_2 (1.0)	25	86	93
12	**C5**	5	CH_3NO_2 (1.0)	45	80	97
13[c]	**C5**	1	CH_3NO_2 (1.0)	45	74	96
14[c]	**C6**	1	CH_3NO_2 (1.0)	45	62	69

[a] Determined by ^{1}H-NMR using mesitylene as internal standard. [b] Determined by HPLC. [c] Reaction time is 5 h.

Table 1 are identical to the observed conversions, and no side products were thus detected.

C5 was then used for further optimization. It was found that enantioselectivity is strongly increased with increased aldehyde concentration as the ee value increased to 91% using a 1M THF solution. Under otherwise identical conditions, in solvents such as toluene, acetonitrile and dichloromethane the reaction efficiency was considerably lower (entries 8–10). Improvements in terms of yield and enantioselectivity were possible using neat nitromethane, still 1M in aldehyde (entry 11). Surprisingly, the enantioselectivity further increased to 97% ee at 45 °C (entry 12). Lowering the catalyst loading from to 5 to 1 mol% and the reaction time from 20 to 5 h only slightly affected productivity and enantioselectivity (entry 13).

Diastereomeric catalyst **C6** was also studied under these optimized conditions (Table 1, entry 14), but was again found to be inferior (ee = 69%, yield = 62%). This mismatch situation also indicates that the axial chirality element is the most important control factor for the stereochemical outcome, as the major enantiomer's absolute configuration stays the same.

Scope

With the optimized conditions, the applicability to other substrates was probed (Table 2). It was found that there is no obvious trend regarding the electronic and steric properties of the substituents on aromatic aldehydes. Independently of *ortho*-, *meta*- and *para*-substitution, high enantioselectivity was attained (entries 4–13). Similarly, σ-donors, π-donors and σ-acceptors were well tolerated. A limitation was found for a π-acceptor substituent reported in entry 14. In this case the yield was high, but the ee value was only 70%. Next to extended π-systems within the aldehyde (entries 1 and 2), also electron rich 2- and 3-furyl moieties were well accommodated (entries 15 & 16).

Of particular note is the applicability to aliphatic sterically hindered aldehydes like pivalic aldehyde (entry 17)[51,115] but also to enolizable, small linear aldehydes such as butanal (entry 18),[31–33,35,51,115] which are to prone to side reactions like aldol condensations. Even more challenging is phenylacetalde-

Table 2 Application of the title reaction to various substrates

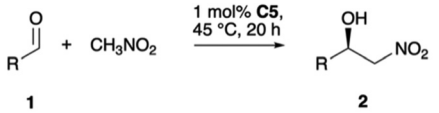

#	R	1/2	Yield[a]/%	ee[b]/%
1	2-Naphthyl	**a**	74	96
2	1-Naphthyl	**b**	71	89
3	Ph	**c**	78	86
4	2-Me-C_6H_4	**d**	84	92
5	3-Me-C_6H_4	**e**	91	94
6	4-Me-C_6H_4	**f**	51	90
7	2-MeO-C_6H_4	**g**	92	94
8	3-MeO-C_6H_4	**h**	80	90
9	4-MeO-C_6H_4	**i**	64	94
10	4-F-C_6H_4	**j**	71	87
11	4-Cl-C_6H_4	**k**	69	80
12	4-Br-C_6H_4	**l**	87	89
13	4-I-C_6H_4	**m**	91	95
14	4-NC-C_6H_4	**n**	94	70
15	2-Furyl	**o**	79	90
16	3-Furyl	**p**	83	93
17	*t*Bu	**q**	72	81
18	*n*Pr	**r**	87	83
19	$PhCH_2$	**s**	93	94

[a] Yield of isolated product. [b] Determined by HPLC.

hyde **1s** (entry 19),[84] due to the double activated α-position. Under the mild conditions provided by the Co(II)-triazolium/naphthoxide catalyst **C5**, it also underwent clean nitroaldol addition without observable side reactions. This underscores the functional group compatibility of the catalyst system.

In addition, we studied the use of 1-nitropropane in order to generate two stereocenters (Table 3). Useful to high yields of isolated **3** were attained using 1 mol% of **C5** at −20 °C for 20 h, with moderate preference for the *syn*-diastereomer (69 : 31–81 : 19) which was formed with good to high enantioselectivity (ee 80–94%).[116,117]

Mechanistic studies

Control experiments. To determine which moieties in the polyfunctional catalyst systems are essential for high performance, a number of control catalyst systems **CC1–CC7** was investigated (Table 4).

In **CC1**, the naphthoxide base is missing and formally replaced by a methyl ether unit (entry 1). In that case, no product was found. By addition of catalytic amounts of Cs_2CO_3 as external base, activity was regained, but racemic product was formed. Notably, when only Cs_2CO_3 was used without any catalyst, considerable background reactivity was found, leading to 33% conversion under the same conditions. Similarly, catalyst **CC2** lacking an azolium side arm,[118–120] gave racemic product in the presence of the external base. The organocatalytic betaine control system **CC7** also formed racemic product in good yield, however in contrast to all other cases shown here, there was a significant difference between conversion and yield. Combining **CC2** and **CC7** to a binary catalyst system resulted in improved yield and a clean transformation, but also here a racemate was obtained.

Like our standard catalyst **C5**, complex **CC3** is a polyfunctional Lewis acid/betaine catalyst. In that case the axially chiral binaphthyl unit is missing, causing a strong loss of enantioselectivity. **CC4** contains a binaphthyl unit, but the azolium is formally replaced by an ether bridge. For activity, the base was necessary again and the product was racemic.

Table 3 Application of the title reaction to form two stereocenters

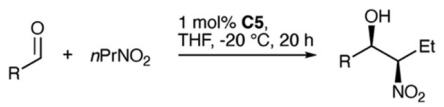

1 **3**

#	R	1/3	Yield[a]/%	*syn* : *anti*	ee(*syn*)[b]/%
1	2-Naphthyl	**a**	74	69 : 31	93
2	Ph	**c**	69	70 : 30	80
3	4-Me-C_6H_4	**f**	81	74 : 26	86
4	4-MeO-C_6H_4	**i**	67	75 : 25	88
5[c]	4-Br-C_6H_4	**l**	84	81 : 19	94
6[c]	4-I-C_6H_4	**m**	86	80 : 20	91

[a] Yield of isolated product. [b] Determined by HPLC. [c] 1.0 M THF was used.

Table 4 Study of control catalysts **CC** in the title reaction

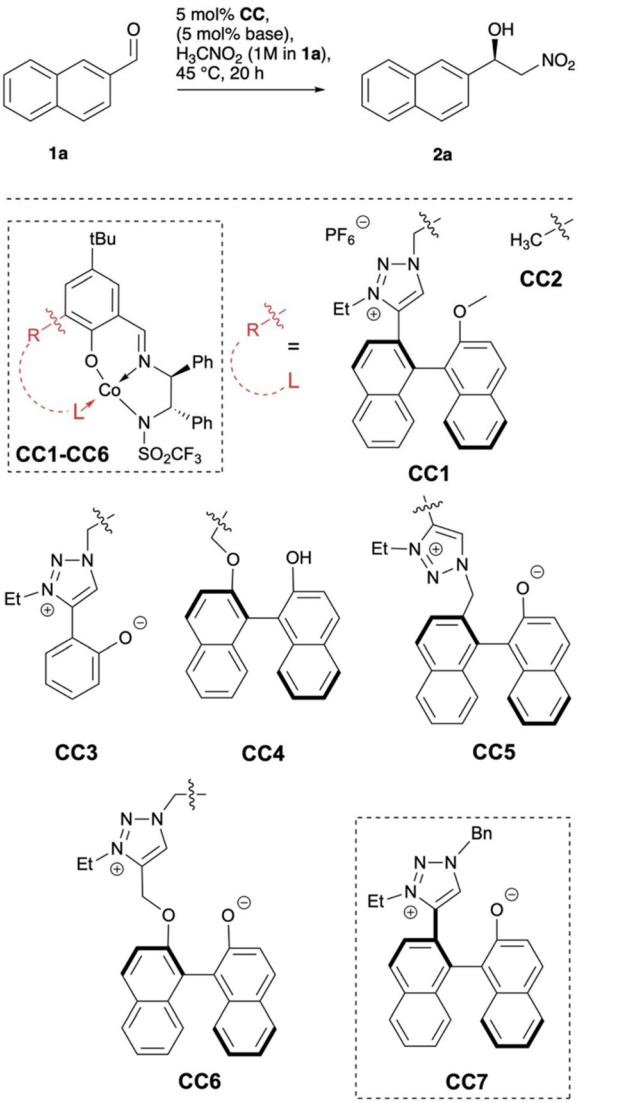

#	CC	External base	Conversion[a]/%	Yield[a]/%	ee[b]/%
1	**CC1**	—	<2	<2	—
2	**CC1**	Cs_2CO_3	90	90	*rac*
3	**CC2**	Cs_2CO_3	71	71	*rac*
4	**CC7**	—	96	82	*rac*
5	**CC2** + **CC7**	—	92	92	*rac*
6	**CC3**	—	70	67	21
7	**CC4**	Cs_2CO_3	80	80	*rac*
8	**CC5**	—	83	83	−7
9	**CC6**	—	32	32	19

[a] Determined by ^{1}H-NMR using mesitylene as internal standard. [b] Determined by HPLC.

CC5 and **CC6** are both betaine catalysts featuring triazolium moieties and axial chirality in the aryloxide part, in which the conformational flexibility is increased compared to **C5** by methylene and methylene ether linkers between the azolium and the binaphthyl fragments. In addition, in **CC5**, the triazo-

lium is connected by a C,C-bond to the phenoxyimine ligand. In both case enantioselectivity was found to be low.

The results of the control experiments are suggesting that a well-balanced spatial fit between all the key functional groups of the catalyst, *i.e.*, chiral Lewis acid sphere, azolium and aryloxide and the functional units of the activated substrates is required for high enantioselectivity.

Kinetic investigation. The empirical rate law was determined using the variable time normalization analysis (VTNA) by Burés (see SI, chapter 3.1).[121–123] This method allowed to elucidate the kinetic orders with respect to all components involved in the model reaction. Kinetic analysis was performed by monitoring the conversion of **1a** by ^{1}H-NMR spectroscopy using catalyst **C5** in THF-d_8. The best fit was found with eqn (1):

$$r = k_{obs}\ [\mathbf{C5}]^{0.90}\ [\mathbf{1a}]^{1.08}\ [MeNO_2]^{0.85} \quad (1)$$

The results thus show a first-order dependence on the catalyst concentration, suggesting that a single catalyst molecule is likely involved in the turnover-determining step(s). A nonlinear effect (NLE)[124,125]study (see SI, chapter 3.3) revealed a linear relationship between the enantiomeric excess (ee) of catalyst **C5** and that of the product **2a**, supporting that higher-order catalyst aggregates are not involved.

The reaction rate also showed a first-order dependence on the aldehyde (**1a**) substrate and a nearly first-order dependence on nitromethane (**NM**) (reaction order = 0.85). This rate law is in good agreement with the energy profile of the calculated mechanism (see below).

Spectroscopic investigations. UV–Vis studies employing Beer's law analysis also support a monomeric catalyst structure in THF (see SI, chapter 3.4.1).

The properties of paramagnetic catalyst **C5** and its precatalyst (featuring the neutral naphthol unit) were investigated using magnetometry and spectroscopy in both the solid state and in solution, to gain insights into their electronic structure and derive implications regarding the catalytic mechanism.

SQUID (superconducting quantum interference device) magnetometry measurements were conducted on powder samples of **C5** and its precatalyst **C5*HPF$_6$**. The room temperature $\chi_m T$ value for the precatalyst **C5*HPF$_6$** was 2.3 cm^3 mol^{-1} K (Fig. S15), which agrees well with the value expected for a spin $S = 3/2$ and $g_{iso} = 2.2$. Below 70 K, the $\chi_m T$ value decreases and reaches 1.5 cm^3 mol^{-1} K at the lowest measurement temperature. This decrease is attributed to sizable zero-field splitting. The temperature dependence of the $\chi_m T$ value for **C5** is qualitatively very similar, but the absolute values are reproducibly lower by 30% (Fig. S16). To assess if this discrepancy is due to lower *g*-values, and to further characterize the compounds, X-band electron paramagnetic resonance (EPR) spectra were recorded on powder samples of the precatalyst C5*HPF$_6$ (Fig. S17) and **C5** (Fig. S18) at 4 K. The spectra are qualitatively very similar and consistent with excitations within the lowest Kramers doublet, where the combined action of *g*-value anisotropy and zero-field splitting leads to a rhombic shape. The combined fit of EPR and SQUID data gave the spin Hamiltonian parameters reported in Table 5. The *g*-tensor values for **C5** and its precatalyst are very similar and the discrepancy between the $\chi_m T$ values of **C5** and its precatalyst can therefore not be due to differences in *g*-values. Therefore, we attribute the difference to the presence of a small amount of a diamagnetic cobalt(III) species formed in the activation process.

UV-Vis measurements on **C5** (2 mM) were carried out to investigate the dependence of the ligand field splitting of the Co(II) center on solvents and substrates. The room temperature UV/Vis spectrum of **C5** in non-coordinating DCM displays two overlapping low-energy bands centered at around at 16 740 and 18 000 cm^{-1}, respectively, that are assigned to dd-transitions (Fig. S11). The spectrum in pure nitromethane displays slightly lower intensities of the above bands, with slightly changed intensity ratio in favour of the high-energy component. Interestingly, the spectrum in pure THF displays an additional band at the lower energy of 14 188 cm^{-1}. Addition of the aldehyde **1a** to the last solution results in insignificant changes, demonstrating that **1a** coordinates less strongly than THF (and the other ligands). However, addition of 1000 eq. of nitromethane to a THF solution causes the disappearance of the lowest-energy absorption band, indicating that nitromethane displaces THF in this case. Coordination of nitromethane to metal centers is known and the ligand field strength is similar to that of water.[126,127]

By means of circular dichroism CD spectroscopy, it is possible to probe the influence of chirality on electronic transitions that involve the metal center. CD-spectra (Fig. S12–S14) recorded in the area of 380 nm (27 000 cm^{-1}) at room temperature reveal negligible intensities for the precatalyst and for the free binaphthol ligand. In contrast, clear CD intensity was observed for **C5** (0.2 mM in DCM), indicating that the relevant electronic transition must involve both the metal and the (chiral) ligand. Therefore, the absorption band is assigned to a charge transfer transition. Addition of nitromethane leads to a small, but significant change in intensity, which could point toward partial dissociation of the naphthoxide moiety from the metal center. Addition of aldehyde does not lead to a measurable change in intensity of the relevant band, but the situation is complicated by strong absorption of the substrate at slightly shorter wavelengths.

DFT calculations. To gain deeper insight into structural properties of the catalyst **C5** and to elucidate the mechanism of the catalytic reaction, we performed DFT calculations at the

Table 5 Spin Hamiltonian parameters derived from SQUID and EPR for **C5** and its precatalyst

Spin Hamiltonian parameters	**C5*HPF$_6$**	**C5**
g_1	2.295(2)	2.54(3)
g_2	2.228(3)	2.22(5)
g_3	2.098(3)	2.21(2)
D (cm^{-1})	28.0(5)	28.2(6)
E/D	0.250(8)	0.258(9)

B3LYP-D3(BJ)/def2-TZVP/COSMO (nitromethane) level of theory, using geometries optimized at the PBEh-3c-D3(BJ)/def2-mSVP level.[128–138] The barrier for the uncatalyzed reaction as determined by DFT is 239.1 kJ mol^{-1} relative to the free reactants. The high calculated barrier along with the lack of enantioselectivity rules out a significant amount of uncatalyzed background reaction.

As no crystal structure of **C5** is available, a model was constructed manually based on calculated geometries of a similar catalytic system.[108,109,113,114] That structure was optimized and served as starting point for all subsequent calculations. In accordance with magnetic measurements identifying the active species as a high-spin Co(II) complex, the reaction pathway was computed with a spin multiplicity of 4.

To investigate the following proposed reaction mechanisms, we computed all relevant stationary points along the reaction pathway, including minima and transition state structures. Building on previous investigations, we propose two possible catalytic cycles, illustrated in Schemes 2 and 3.

The first mechanism, here referred to as the *standard mechanism*, follows the common pathway for polyfunctional Lewis acid/azolium–aryloxide betaine catalysts.[108,113,114] Here, the pronucleophile is deprotonated by the naphthoxide base and the resulting nucleophile stabilized by a metal center, in our case cobalt(II). In this mechanism, the electrophile is activated by the resulting azolium naphthol moiety *via* H-bonding. Based on the pK_a values of nitromethane (pK_a = 10.2 at 25 °C)[139] and 2-naphthol (pK_a = 9.5 at 25 °C)[139,140] in water, the deprotonation step is expected to be slightly endergonic, a finding that is also consistent with the DFT calculations presented in Fig. 1.

In the proposed *inverse mechanism*, the naphthoxide base also deprotonates the nitromethane leading to a nitronate which is further stabilized by coordination to the metal center and by hydrogen bonding to the naphthol OH generated during the proton transfer. In that case, the aldehyde also binds to the metal center, which distinguishes the *inverse* from the *standard* pathway.

In neither mechanism does the catalyst exist in its bare activated form, but it is generally interacting with a nitromethane molecule as depicted in **I** in Scheme 2.

The interaction is further facilitated by the use of nitromethane as solvent, but the association is also energetically favourable, as the binding of nitromethane to the catalyst is exothermic. It involves a H-bond between the azolium and the nitro group, which further acidifies the nitromethane, which, at the same time, is exposing its methyl unit to the basic naphtholate unit. In the energetically lowest starting structure **I** visualized in Fig. 2, the cobalt center adopts a highly distorted tetrahedral coordination geometry, as indicated by the O–Co–N angle of 124° between the binaphthyl-O, the Co(II) and the adjacent N atom.

The catalytic cycle of the *standard mechanism* is depicted in Scheme 2 and the Gibbs energy along the cycle as obtained by DFT is shown in Fig. 1. The cycle begins with the deprotonation of nitromethane by the binaphtholate. The resulting nitronate anion is stabilized by a H-bond to the binaphthyl-OH, which was generated during the proton transfer, yielding intermediate **II$_s$**. During the deprotonation, the bond between the Co center and the naphthoxide-O is broken, which is supported by UV/VIS spectroscopy. After adding nitromethane to the catalyst, the charge-transfer band associated with the Co–O bonding diminishes by 20%, indicating a cleavage of this bond. The barrier for the deprotonation from **I** to **II$_s$** was found to be 92.0 kJ mol^{-1} with respect to **I**, see Fig. 1. The coordination geometry of Co remains largely unchanged except for replacing the naphthoxide-O by a nitronate-O atom.

In the subsequent step of the catalytic cycle, from **II$_s$** to **III$_s$**, the aldehyde undergoes a H-bond formation with the naphthol moiety, thus cleaving the H-bond between naphthol and nitronate. Instead, both oxygen atoms of the nitronate

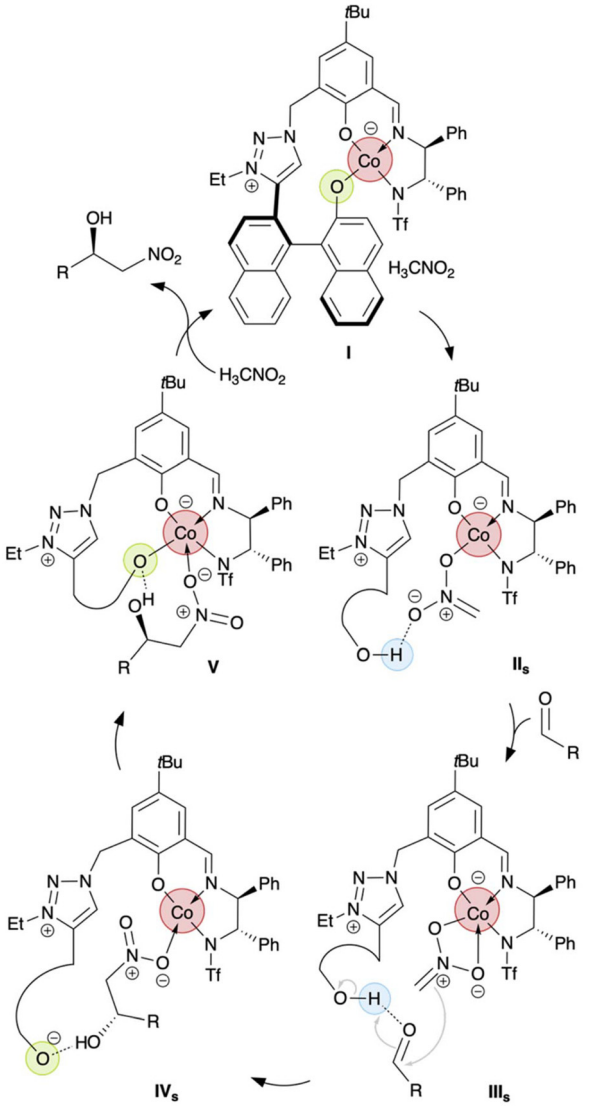

Scheme 2 Proposed catalytic cycle for the *standard mechanism*. Like in Scheme 1, red circles indicate a Lewis acid, green circles a Brønsted base, and blue circles a H bond donor participating in the individual steps.

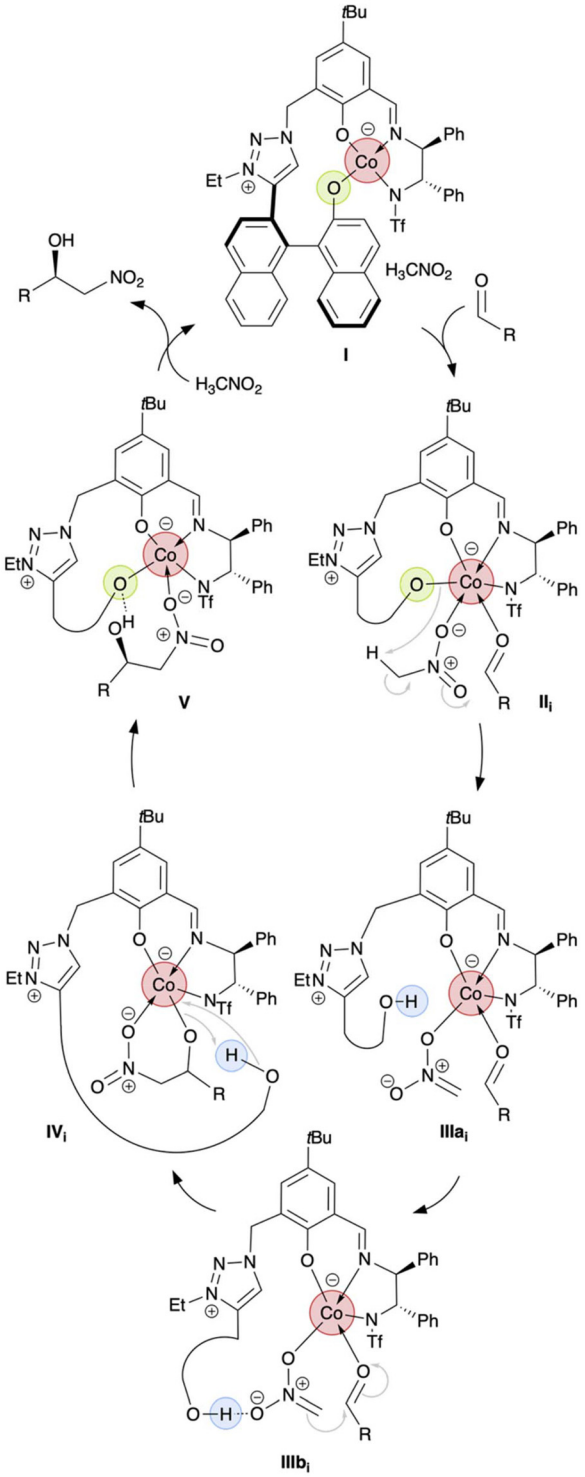

Scheme 3 Proposed catalytic cycle of the *inverse mechanism*. Like in Scheme 1, red circles indicate a Lewis acid, green circles a Brønsted base, and blue circles a H bond donor participating in the individual steps.

now function as a bidentate ligand to the Co center, forming intermediate $\mathbf{III_s}$. At the same time, the coordination environment of Co shifts from a distorted tetrahedral geometry to a very distorted square pyramidal arrangement.

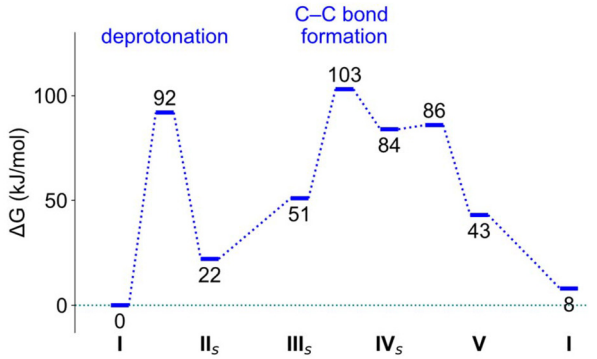

Fig. 1 Free energy profile of the *standard mechanism*. The catalyst **C5**/nitromethane adduct **I** was chosen as reference state.

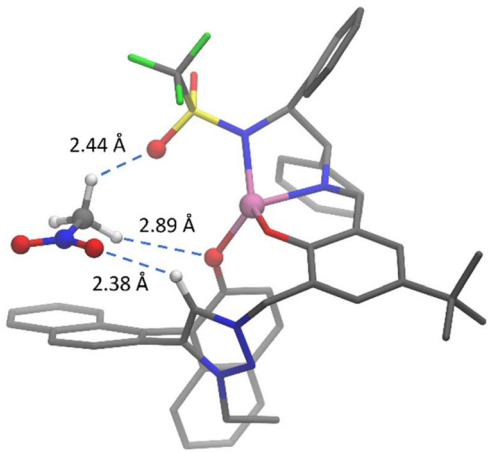

Fig. 2 Molecular structure of species **I** which is the starting geometry of both proposed reaction mechanisms. Nitromethane forms weak hydrogen bonds to the active catalyst. Important distances are highlighted.

The following C–C bond formation step from $\mathbf{III_s}$ to $\mathbf{IV_s}$ is stereo-determining as the corresponding transition state has the highest energy in the catalytic cycle, 102.8 kJ mol^{-1} (see Fig. 1 and Fig. 3, top). The transition state forming the unfavored (*S*)-enantiomer is visualized in Fig. 3 (bottom) and found at a significantly higher energy of 115.2 kJ mol^{-1}, resulting in a computed ee of 98%, which is in close agreement with the experimental value of 97%. The higher energy of the (*S*)-transition state may be attributed to a weaker H-bond between the aldehyde substrate and the naphthol, with a distance of 1.55 Å compared to 1.46 Å in the transition state leading to the favored (*R*)-enantiomer.

In addition, the hydrogen bonding atoms in the (*S*)-transition state deviate more from a linear geometry, showing an angle of 169.2° *versus* 173.5° for the (*R*)-transition state (see Fig. 3). Simultaneously, upon the C–C bond formation, the

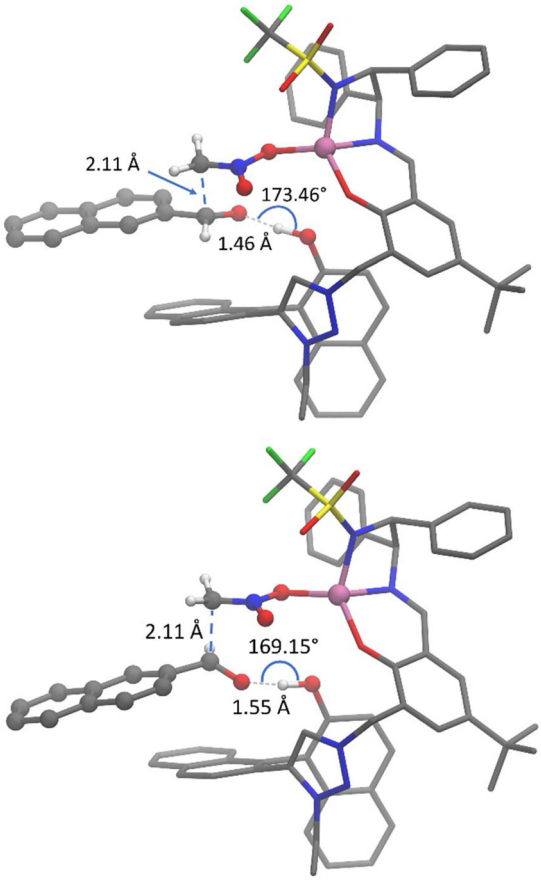

Fig. 3 Comparison of the transition states leading to the favored (*R*) (top) and disfavored (*S*) (bottom) enantiomers in the C–C bond formation from $\mathbf{III_s}$ to $\mathbf{IV_s}$ in the *standard mechanism*. Most H atoms are omitted for clarity. White: H, gray: C, pink: Co, red: O, blue: N, yellow: S, green: F.

resulting alkoxide is protonated intramolecularly by the naphthol moiety. In intermediate $\mathbf{IV_s}$, the cobalt coordination sphere returns to a distorted tetrahedral geometry, similar to **I**. In the second to last step, *i.e.*, from $\mathbf{IV_s}$ to **V**, the bond between Co and the naphtholate-O is formed again to yield intermediate **V**. Finally, the neutral product is released from the complex and a new nitromethane molecule binds to the catalyst, formally completing the catalytic cycle. Although no transition state for the last step was identified, relaxed surface scans suggest a low barrier, consistent with the predictions from microkinetic modelling which will be further explained below.

In the *inverse mechanism*, the first intermediate (**I**) is identical to that of the *standard mechanism* (Scheme 3). The initial step is the coordination of the aldehyde to the Co center to form intermediate $\mathbf{II_i}$, which is in contrast to the *standard* pathway where it binds to the binaphthyl-OH moiety. In $\mathbf{II_i}$, an octahedral coordination is found, as the nitroolefin also coordinates to the metal center. The following step is the deprotonation of the coordinating nitromethane, yielding intermediate $\mathbf{IIIa_i}$ *via* a transition state with an energy of 110.5 kJ mol^{-1} (Fig. 4). This is followed by the formation of a H-bond between

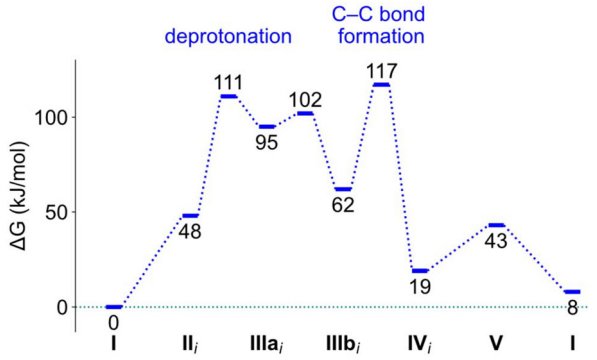

Fig. 4 Free energy profile of the *inverse mechanism*. **I** was chosen as reference state.

the nitronate and the naphthol unit in $\mathbf{IIIb_i}$ with a relative energy of 102.2 kJ mol^{-1}. In structures $\mathbf{IIIa_i}$ and $\mathbf{IIIb_i}$, the cobalt has a square pyramidal coordination environment, as the bond between the binaphthyl-O and Co becomes elongated, while the bond to the nitronate is shortened. In $\mathbf{IIIb_i}$ and the subsequent intermediate $\mathbf{IV_i}$, the key difference between the two mechanisms becomes evident: in this alternative option, the aldehyde coordinates to the Co center rather than forming a H-bond to the naphthol's OH that is observed in the *standard mechanism*. Furthermore, the nitronate is simultaneously binding to both the Co center and the binaphthyl-OH in the *inverse mechanism*.

The C–C bond formation from $\mathbf{IIIb_i}$ to $\mathbf{IV_i}$ proceeds through the turnover determining transition state (TDTS, Fig. 5) with the highest energy of the catalytic cycle (117.0 kJ mol^{-1}, see Fig. 4). Since the turnover determining intermediate is **I** with a relative energy of 0 kJ mol^{-1}, the energetic span is also 117.0 kJ mol^{-1}.

In addition to the C–C bond formation, the shift of a H-bond from stabilizing the nitronate to stabilizing the newly

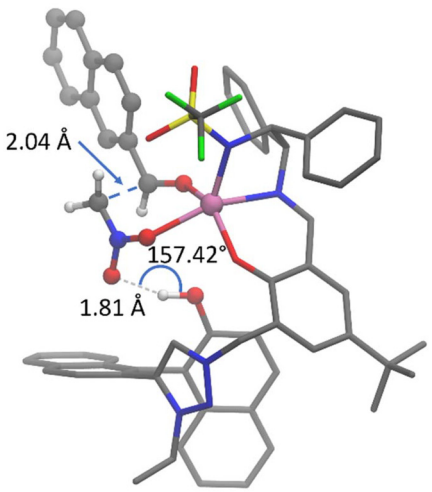

Fig. 5 Transition state of the C–C bond formation from $\mathbf{IIIb_i}$ to $\mathbf{IV_i}$ for the *inverse mechanism*. Most H atoms are omitted for clarity.

formed alkoxide occurs in the same step, thereby changing the coordination sphere of Co to a trigonal bipyramidal geometry.

Subsequently, the alkoxide is protonated by the naphthol while the resulting naphthoxide binds to Co again and the product's OH is released from the metal center to give intermediate **V**. Product release and association of nitromethane to the catalyst closes the catalytic cycle.

To conclude, the rate-limiting barrier of the *standard mechanism* is calculated to be 14.2 kJ mol^{-1} lower than that of the *inverse mechanism*. Thus, a preference for the *standard* pathway is likely and in good agreement with the microkinetic modelling (see below).

Microkinetic modelling. Microkinetic modelling allows direct comparison of Gibbs free energies obtained from DFT calculations and experimental kinetic data. The kinetic model comprises a reaction network, *i.e.*, a set of elementary reactions (Table 6) and their rate constants. Solving the kinetic equations results in the concentrations of all species involved over time.[141–143] The rate constants were optimized to match the experimental concentration profiles over time for several different initial conditions. Fig. S19 and S20 in the SI show a comparison of the experimental aldehyde (**1a**) and product concentration profiles and the simulation results of the microkinetic model. From the optimized rate constants, activation barriers were calculated (Table 6) and compared directly with the DFT barriers of the standard mechanism, as presented in Fig. 6. The agreement is satisfactory: DFT predicts the two highest barriers to be larger than the kinetic model, by 10.0 kJ mol^{-1} for the deprotonation of nitromethane and 13.0 kJ mol^{-1} for the C–C formation. The difference to the highest barrier in the inverse mechanism would be 27.2 kJ mol^{-1}, indicating once more that the *standard* mechanism is likely to occur.

The concentration profiles of the aldehyde and product were measured experimentally under four different conditions. The initial concentrations (Table 1, entry 13) of the reaction were varied by increasing either the aldehyde or the catalyst concentrations. In an additional experiment, the catalyst was pre-stirred in nitromethane for 5 h hours before the increased amount of aldehyde was added. The pre-stirring experiment was designed to investigate the possibility of catalyst decay. Comparing the concentration profiles with and without pre-stirring shows that pre-stirring significantly slows down the reaction, which suggests that the catalyst decays over time. Consequently, catalyst decay was included as an elementary step in the reaction network (Table 6). Simulations indicate that 41% of the catalyst decays after 5 h of pre-stirring. The decay product has not yet been identified.

However, it should be noted that the model is not unique, and that alternative parameters and reaction networks can also fit the experimental data equally well for the standard mechanism (Fig. 6, gray). Only the sensitive barriers (**I** to **II$_s$** and **III$_s$** to **V**) can be precisely determined, while others vary widely without affecting the fit quality. Nevertheless, the model is in close agreement with the experimental and DFT data, suggesting that the reaction network is plausible.

Table 6 All the elementary reactions used to model the catalytic cycle are listed. The Gibbs free energy barriers are obtained from the microkinetic model in kJ mol^{-1}

Elementary reaction	$\Delta G^{\ddagger}$ forward (kJ mol^{-1})	$\Delta G^{\ddagger}$ backward (kJ mol^{-1})
I ↔ **II$_s$**	82.0	61.5
II$_s$ + RCHO ↔ **III$_s$**	40.8	13.8
III$_s$ ↔ **V**	42.2	70.0
V + H_3CNO_2 ↔ **I** + product	14.8	33.8
II$_s$ → side product	85.2	—

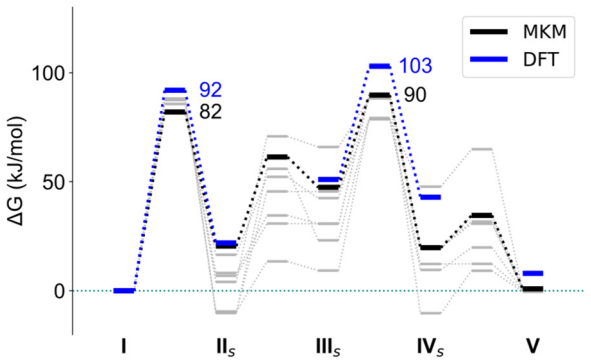

Fig. 6 The reaction barriers from the microkinetic model (gray, black) and DFT barriers (blue) for the standard mechanism are compared. Multiple sets of barriers in the microkinetic model reproduce the experimental concentration profiles equally well. The set of barriers that best agrees with the DFT barriers is highlighted in black and was used for the simulation shown in Fig. S19 and S20 (SI).

Conclusions

The development of polyfunctional catalysts opens new opportunities for mimicking the efficiency of enzymes in asymmetric transformations. In this context, we presented a novel approach to the nitroaldol reaction that relies on a catalyst system combining cobalt(II) as a Lewis acid with an azolium–aryloxide betaine. This catalyst displays mechanistic features reminiscent of class-II aldolases, where several functional elements cooperate to achieve high stereocontrol.

DFT calculations, microkinetic simulations, and spectroscopic studies provided deep insight into how the catalyst most likely operates. The cobalt(II) center contributes Lewis acidity (like in class-II-aldolases Zn(II), Co(II) *etc.*), the aryloxide moiety functions as a Brønsted base (like in class-II-aldolases usually glutamate), while the corresponding aromatic alcohol derived from it plays a dual role: as a hydrogen-bond donor and as a Brønsted acid (like in class-II-aldolases usually tyrosine). Together, these functions create a chiral highly orchestrated reaction environment, in which bond activation, stabilization of intermediates and transition states, and stereochemical control are precisely balanced. Remarkably, for nitro-

methane this cooperative interplay allows the reaction to proceed with excellent stereoselectivity even at slightly elevated temperatures.

Beyond its mechanistic mode of action, the practical advantages of this system are noteworthy. Because no external base is required and the participating functional groups of the catalyst are only weakly acidic and basic, the conditions are very mild minimizing competing side reactions.[144–146] As a result, the scope of the reaction extends to readily enolizable aldehydes, including substrates such as phenylacetaldehyde, which are problematic in classical nitroaldol protocols.

Thus, this polyfunctional catalyst design not only provides a new route to stereoselective nitroaldol reactions, but also demonstrates carefully integrated catalytic elements matching the multifaceted strategies of enzymatic systems.

Author contributions

K. J. planned and conducted the catalytic and kinetic experiments and carried out the catalyst syntheses. L. A. S. performed all DFT calculations and the microkinetic modeling. A. A. and R. K. planned the spectroscopic studies. A. A., R. K. and S. M. performed the spectroscopic investigations. J. v. S. directed the spectroscopic studies. J. K. directed the DFT calculations and the microkinetic modelling. R. P. conceptualized and directed the project. R. P., K. J., L. A. S., A. A. and R. K. wrote the manuscript. All authors contributed to the discussion.

Conflicts of interest

There are no conflicts to declare.

Data availability

The data that support the findings of this study are available in the supplementary information (SI) of this article.

Supplementary information is available. See DOI: **https://doi.org/10.1039/d5qo01558h**.

Acknowledgements

This work was financially supported by the Deutsche Forschungsgemeinschaft (DFG, project ID 310990893 – PE 818/7-2; project ID 358283783 – CRC 1333/2, project ID 516238647 – CRC 1667/1 - ATLAS). The authors acknowledge support by the state of Baden-Württemberg through bwHPC and the German Research Foundation (DFG) through grant no INST 40/575-1 FUGG (JUSTUS 2 cluster). K. J. acknowledges financial support in the form of a PhD BMBF scholarship by the Friedrich-Naumann-Foundation (FNF). L. A. S. acknowledges financial support in the form of a Ph.D. scholarship from the Studienstiftung des Deutschen Volkes (German National Academic Foundation).

References

1 L. Henry, Formation synthétique d'alcools nitrés, *Bull. Soc. Chim. Fr.*, 1895, **13**, 999–1002.
2 R. S. Varma, R. Dahiya and S. Kumar, Microwave-assisted Henry reaction: solventless synthesis of conjugated nitroalkenes, *Tetrahedron Lett.*, 1997, **38**, 5131–5134.
3 N. Ono, *The Nitro Group in Organic Synthesis*, John Wiley & Sons, 2003.
4 R. Ballini, New and convenient synthesis of (*Z*)-heneicos-6-en-11-one, the douglas fir tussock moth (*Orgyia pseudotsugata*) sex pheromone, and (*Z*)-non-6-en-2-one, the immediate precursor for the synthesis of brevicomin, the sex attractant of the western pine beetle *Dentroctonus brevicomis*, *J. Chem. Soc.*, 1991, 1419–1421.
5 W. E. Noland, The NEF reaction, *Chem. Rev.*, 1955, **55**, 137–155.
6 P. B. Kisanga and J. G. Verkade, $P(RNCH_2CH_2)_3N$: An Efficient promoter for the nitroaldol (Henry) reaction, *J. Org. Chem.*, 1999, **64**, 4298–4303.
7 R. J. Heffner, J. Jiang and M. M. Joullie, Total synthesis of (-)-nummularine F, *J. Am. Chem. Soc.*, 1992, **114**, 10181–10189.
8 C. Palomo, M. Oiarbide and A. Laso, *Eur. J. Org. Chem.*, 2007, 2561–2574.
9 O. Sakanaka, T. Ohmori, S. Kozaki and T. Suami, Recent advances in the catalytic asymmetric nitroaldol (Henry) reaction, *Bull. Chem. Soc. Jpn.*, 1986, **59**, 3523–3528.
10 T. Suami, H. Sasai and K. Matsuno, Synthesis of methyl hexaacetyl-tunicaminyl uracil, *Chem. Lett.*, 1983, **12**, 819–822.
11 G. Mikite, E. Jakucs, A. Kis-Tamás, F. Darvas and A. Lopata, Synthesis and antifungal activity of new nitro–alcohol derivatives, *Pestic. Sci.*, 1982, **13**, 557–562.
12 T. Yasuhara, N. Zaima, S. Hashimoto, M. Yamazaki and O. Muraoka, First total synthesis of crispin B by nitro Aldol and the Bischler-Napieralski reaction, *Heterocycles*, 2009, **77**, 1397.
13 K. Sato, S. Akai, H. Shoji, N. Sugita, S. Yoshida, Y. Nagai, K. Suzuki, Y. Nakamura, Y. Kajihara and M. Funabashi, Stereoselective and efficient total synthesis of optically active Tetrodotoxin from d-glucose, *J. Org. Chem.*, 2008, **73**, 1234–1242.
14 Y. Li, J. P. Feng, W. H. Wang, J. Chen and X. P. Cao, Total synthesis and correct absolute configuration of malyngamide U, *J. Org. Chem.*, 2007, **72**, 2344–2350.
15 J. Boruwa and N. C. Barua, Stereoselective total synthesis of (+)-boronolide, *Tetrahedron*, 2006, **62**, 1193–1198.
16 M. E. Bunnage, S. G. Davies, C. J. Goodwin and O. Ichihara, An expeditious asymmetric synthesis of allophenylnorstatine, *Tetrahedron*, 1994, **50**, 3975–3986.

17 U. Veith, O. Schwardt and V. Jäger, Concise synthesis of deacetylanisomycin and 2-substituted analogues from N, 2-O-Dibenzyl-L-threose imine1, *Synlett*, 1996, 1181–1183.
18 P. M. Koskinen and A. M. P. Koskinen, Sphingosine, an enigmatic lipid: a review of recent literature syntheses, *Synthesis*, 1998, 1075–1091.
19 D. Lednicer and L. A. Mitscher, *The Organic Chemistry of Drug Synthesis*, John Wiley & Sons, 1980, vol. 2.
20 N. Shibata, T. Katoh and S. Terashima, An expeditious synthesis of (2R, 3S)-3-tert-butoxycarbonylamino-1-isobutylamino-4-phenyl-2-butanol, a key building block of HIV protease inhibitors, *Tetrahedron Lett.*, 1997, **38**, 619–620.
21 T. Kumamoto, N. Aoyama, S. Nakano, T. Ishikawa and S. Narimatsu, Synthesis of enantiomeric 4-hydroxypropranolols from 1, 4-dihydroxynaphthalene, *Tetrahedron: Asymmetry*, 2001, **12**, 791–795.
22 J. B. Hickie, Alprenolol ("APTIN") in Angina pectoris a double-bund multicentre trial, *Med. J. Aust.*, 1970, **2**, 268–272.
23 M. R. Candelore, L. Deng, L. Tota, X. M. Guan, A. Amend, Y. Liu, R. Newbold, M. A. Cascieri and A. E. Weber, Potent and selective human β3-adrenergic receptor antagonists, *J. Pharmacol. Exp. Ther.*, 1999, **290**, 649–655.
24 M. J. Kendall and V. A. John, Oxprenolol: Clinical pharmacology, pharmacokinetics, and pharmacodynamics, *Am. J. Cardiol*, 1983, **52**, D27–D33.
25 H. M. Krumholz, β-blockers for mild to moderate heart failure, *Lancet*, 1999, **353**, 2–3.
26 K. Tekes, P. Szegi, F. Hashemi, R. Laufer, H. Kalász, A. Siddiq and C. Ertsey, Medicinal chemistry of antimigraine drugs, *Curr. Med. Chem.*, 2013, **20**, 3300–3316.
27 V. A. Cullum, J. B. Farmer, D. Jack and G. P. Levy, Salbutamol: a new, selective β–adrenoceptive receptor stimulant, *Br. J. Pharmacol.*, 1969, **35**, 141–151.
28 K. K. Chen and C. F. Schmidt, The action of ephedrine, the active principle of the Chinese drug Ma Huang, *J. Pharmacol. Exp. Ther.*, 1924, **24**, 339–357.
29 A. J. Coleman, W. P. Leary and A. C. Asmal, The cardiovascular effects of etilefrine, *Eur. J. Clin. Pharmacol.*, 1975, **8**, 41–45.
30 D. C. Harrison, C. A. Chidsey and E. Braunwald, Studies on the mechanism of action of metaraminol (Aramine), *Ann. Intern. Med.*, 1963, **59**, 297–305.
31 M. Shibasaki and N. Yoshikawa, Lanthanide complexes in multifunctional asymmetric catalysis, *Chem. Rev.*, 2002, **102**, 2187–2210.
32 H. Sasai, T. Suzuki, S. Arai, T. Arai and M. Shibasaki, Basic character of rare earth metal alkoxides. Utilization in catalytic carbon-carbon bond-forming reactions and catalytic asymmetric nitroaldol reactions, *J. Am. Chem. Soc.*, 1992, **114**, 4418–4420.
33 M. Shibasaki, H. Sasai and T. Arai, Asymmetric catalysis with heterobimetallic compounds, *Angew. Chem., Int. Ed. Engl.*, 1997, **36**, 1236–1256.
34 T. Arai, Y. M. A. Yamada, N. Yamamoto, H. Sasai and M. Shibasaki, Self-Assembly of heterobimetallic complexes and reactive nucleophiles: a general strategy for the activation of asymmetric reactions promoted by heterobimetallic catalysts, *Chem. – Eur. J.*, 1996, **2**, 1368–1372.
35 H. Sasai, T. Tokunaga, S. Watanabe, T. Suzuki, N. Itoh and M. Shibasaki, Efficient diastereoselective and enantioselective nitroaldol reactions from prochiral starting materials: utilization of La-Li-6,6′-disubstituted BINOL complexes as asymmetric catalysts, *J. Org. Chem.*, 1995, **60**, 7388–7389.
36 J. Boruwa, N. Gogoi, P. P. Saikia and N. C. Barua, Catalytic asymmetric Henry reaction, *Tetrahedron: Asymmetry*, 2006, **17**, 3315–3326.
37 C. Christensen, K. Juhl, R. G. Hazell and K. A. Jørgensen, Copper-catalyzed enantioselective Henry reactions of α-keto esters: An easy entry to optically active β-nitro-α-hydroxy esters and β-amino-α-hydroxy esters, *J. Org. Chem.*, 2002, **67**, 4875–4881.
38 K. Ma and J. You, Rational design of sterically and electronically easily tunable chiral bisimidazolines and their applications in dual Lewis acid/Brønsted base catalysis for highly enantioselective nitroaldol (Henry) reactions, *Chem. – Eur. J.*, 2007, **13**, 1863–1871.
39 B. Qin, X. Xiao, X. Liu, J. Huang, Y. Wen and X. Feng, Highly enantioselective Henry (nitroaldol) reaction of aldehydes and α-ketoesters catalyzed by N, N'-dioxide-copper(I) complexes, *J. Org. Chem.*, 2007, **72**, 9323–9328.
40 M. Bandini, M. Benaglia, R. Sinisi, S. Tommasi and A. Umani-Ronchi, Recoverable PEG-supported copper catalyst for highly stereocontrolled nitroaldol condensation, *Org. Lett.*, 2007, **9**, 2151–2153.
41 Y. Xiong, F. Wang, X. Huang, Y. Wen and X. Feng, A new copper(I)–tetrahydrosalen–catalyzed asymmetric Henry reaction and Its extension to the synthesis of (S)–norphenylephrine, *Chem. – Eur. J.*, 2007, **13**, 829–833.
42 T. Arai, M. Watanabe and A. Yanagisawa, Practical asymmetric Henry reaction catalyzed by a chiral diamine-Cu $(OAc)_2$ complex, *Org. Lett.*, 2007, **9**, 3595–3597.
43 G. Blay, E. Climent, I. Fernández, V. Hernández-Olmos and J. R. Pedro, Enantioselective Henry reaction catalyzed with copper(II)–iminopyridine complexes, *Tetrahedron: Asymmetry*, 2007, **18**, 1603–1612.
44 K. Y. Spangler and C. Wolf, Asymmetric copper(I)-catalyzed Henry reaction with an aminoindanol-derived bisoxazolidine ligand, *Org. Lett.*, 2009, **11**, 4724–4727.
45 G. Blay, L. R. Domingo, V. Hernández-Olmos and J. R. Pedro, New highly asymmetric Henry reaction catalyzed by Cu II and a C1-symmetric aminopyridine ligand, and Its application to the synthesis of miconazole, *Chem. – Eur. J.*, 2008, **14**, 4725–4730.
46 G. Zhang, E. Yashima and W. Woggon, Versatile supramolecular copper(II) complexes for Henry and Aza–Henry reactions, *Adv. Synth. Catal.*, 2009, **351**, 1255–1262.
47 M. Breuning, D. Hein, M. Steiner, V. H. Gessner and C. Strohmann, Chiral 2–endo–substituted 9–oxabispidines: novel ligands for enantioselective copper(II)–catalyzed Henry reactions, *Chem. – Eur. J.*, 2009, **15**, 12764–12769.

48 A. Noole, K. Lippur, A. Metsala, M. Lopp and T. Kanger, Enantioselective Henry reaction catalyzed by CuII salt and bipiperidine, *J. Org. Chem.*, 2010, **75**, 1313–1316.
49 M. Steurer and C. Bolm, Synthesis of amino-functionalized sulfonimidamides and their application in the enantioselective Henry reaction, *J. Org. Chem.*, 2010, **75**, 3301–3310.
50 L. Cheng, J. Dong, J. You, G. Gao and J. Lan, Copper(II)-catalyzed syn-selective Henry reaction, *Chem. – Eur. J.*, 2010, **16**, 6761–6765.
51 I. Panov, P. Drabina, Z. Padelkova, P. Šimůnek and M. Sedlak, Highly enantioselective nitroaldol reactions catalyzed by copper(II) complexes derived from substituted 2-(pyridin-2-yl) imidazolidin-4-one ligands, *J. Org. Chem.*, 2011, **76**, 4787–4793.
52 X. Wang, W. Zhao, G. Li, J. Wang, G. Liu, L. Liu, R. Zhao and M. Wang, Enantioselective copper(II)–catalyzed Henry reaction utilizing chiral aziridinyl alcohols, *Appl. Organomet. Chem.*, 2014, **28**, 892–899.
53 D. Didier, C. Magnier-Bouvier and E. Schulz, Charge–transfer interactions: an efficient tool for recycling bis (oxazoline)–copper complexes in asymmetric Henry reactions, *Adv. Synth. Catal.*, 2011, **353**, 1087–1095.
54 G. Lai, F. Guo, Y. Zheng, Y. Fang, H. Song, K. Xu, S. Wang, Z. Zha and Z. Wang, Highly enantioselective Henry reactions in water catalyzed by a copper tertiary amine complex and applied in the synthesis of (S)-N-trans-Feruloyl octopamine, *Chem. – Eur. J.*, 2011, **17**, 1114–1117.
55 Q. J. Yao, Q. Gao and M. A. J. Zaher, Efficient asymmetric copper(I)–catalyzed Henry reaction using chiral N–alkyl–C1–tetrahydro–1,1′–bisisoquinolines, *Eur. J. Org. Chem.*, 2011, 4892–4898.
56 K. Xu, G. Lai, Z. Zha, S. Pan, H. Chen and Z. Wang, A Highly anti-selective asymmetric Henry reaction catalyzed by a chiral copper complex: applications to the syntheses of (+)-spisulosine and a pyrroloisoquinoline derivative, *Chem. – Eur. J.*, 2012, **18**, 12357–12362.
57 S. Hazra, A. Karmakar, C. Maria de Fátima, L. Dlháň, R. Boča and A. J. L. Pombeiro, Sulfonated Schiff base dinuclear and polymeric copper(II) complexes: crystal structures, magnetic properties and catalytic application in Henry reaction, *New J. Chem.*, 2015, **39**, 3424–3434.
58 D. A. Evans, D. Seidel, M. Rueping, H. W. Lam, J. T. Shaw and C. W. Downey, A new copper acetate-bis (oxazoline)-catalyzed, enantioselective Henry reaction, *J. Am. Chem. Soc.*, 2003, **125**, 12692–12693.
59 S. Saranya, N. A. Harry, S. M. Ujwaldev and G. Anilkumar, Recent advances and perspectives on the zinc–catalyzed nitroaldol (Henry) reaction, *Asian J. Org. Chem.*, 2017, **6**, 1349–1360.
60 B. Zheng, M. Wang, Z. Li, Q. Bian, J. Mao, S. Li, S. Liu, M. Wang, J. Zhong and H. Guo, Asymmetric Henry reaction catalyzed by a Zn–amino alcohol system, *Tetrahedron: Asymmetry*, 2011, **22**, 1156–1160.
61 A. Bulut, A. Aslan and O. Dogan, Catalytic asymmetric nitroaldol (Henry) reaction with a zinc-Fam catalyst, *J. Org. Chem.*, 2008, **73**, 7373–7375.
62 S. Liu and C. Wolf, Asymmetric nitroaldol reaction catalyzed by a C2-symmetric bisoxazolidine ligand, *Org. Lett.*, 2008, **10**, 1831–1834.
63 C. Palomo, M. Oiarbide and A. Laso, Enantioselective Henry reactions under dual Lewis acid/amine catalysis using chiral amino alcohol ligands, *Angew. Chem., Int. Ed.*, 2005, **44**, 3881–3884.
64 B. M. Trost and V. S. C. Yeh, A dinuclear Zn catalyst for the asymmetric nitroaldol (Henry) reaction, *Angew. Chem.*, 2002, **114**, 889–891.
65 R. Kowalczyk, Ł. Sidorowicz and J. Skarżewski, Asymmetric nitroaldol reaction catalyzed by a chromium (III)–salen system, *Tetrahedron: Asymmetry*, 2007, **18**, 2581–2586.
66 A. Zulauf, M. Mellah and E. Schulz, New chiral thiophene– salen chromium complexes for the asymmetric Henry reaction, *J. Org. Chem.*, 2009, **74**, 2242–2245.
67 F. Ibrahim, N. Jaber, V. Guerineau, A. Hachem, G. Ibrahim, M. Mellah and E. Schulz, Recoverable salen-based macrocyclic chiral complexes; catalysts for enantioselective Henry reactions, *Tetrahedron: Asymmetry*, 2013, **24**, 1395–1401.
68 M. M. Islam, P. Bhanja, M. Halder, A. Das, A. Bhaumik and S. M. Islam, Chiral Cr(III)-salen complex embedded over sulfonic acid functionalized mesoporous SBA-15 material as an efficient catalyst for the asymmetric Henry reaction, *Mol. Catal.*, 2019, **475**, 110489.
69 K. Ishihara, Y. Kato, N. Takeuchi, Y. Hayashi, Y. Hagiwara, S. Shibuya, T. Natsume and M. Matsugi, Asymmetric Henry Reaction Using Cobalt Complexes with Bisoxazoline Ligands Bearing Two Fluorous Tags, *Molecules*, 2023, **28**, 7632.
70 Y. L. Wei, K. F. Yang, F. Li, Z. J. Zheng, Z. Xu and L. W. Xu, Probing the evolution of an Ar-BINMOL-derived salen–Co (III) complex for asymmetric Henry reactions of aromatic aldehydes: salan–Cu(II) versus salen–Co(III) catalysis, *RSC Adv.*, 2014, **4**, 37859.
71 K. Lang, J. Park and S. Hong, Urea/transition–metal cooperative catalyst for anti–selective asymmetric nitroaldol reactions, *Angew. Chem., Int. Ed.*, 2012, **51**, 1620–1624.
72 J. Park, K. Lang, K. A. Abboud and S. Hong, Self-assembled dinuclear cobalt(II)-salen catalyst through hydrogen-bonding and its application to enantioselective nitro-aldol (Henry) reaction, *J. Am. Chem. Soc.*, 2008, **130**, 16484–16485.
73 Y. Kogami, T. Nakajima, T. Ikeno and T. Yamada, Enantioselective Henry reaction catalyzed by salen-cobalt complexes, *Synthesis*, 2004, 1947–1950.
74 N. Ananthi, Chiral cobalt complexes synthesised from l-valine: as potential catalysts for asymmetric Henry reaction, *MOJ Biorg. Org. Chem.*, 2017, **1**, 00038.
75 T. Karasawa, N. Kumagai and M. Shibasaki, Heterogeneous heterobimetallic catalysis enabling expedi-

tious access to CF_3-containing vic-amino alcohols, *Org. Lett.*, 2018, **20**, 308–311.

76 T. Karasawa, R. Oriez, N. Kumagai and M. Shibasaki, Anti-selective catalytic asymmetric nitroaldol reaction of α-keto esters: intriguing solvent effect, flow reaction, and synthesis of active pharmaceutical ingredients, *J. Am. Chem. Soc.*, 2018, **140**, 12290–12295.

77 A. Nonoyama, K. Hashimoto, A. Saito, N. Kumagai and M. Shibasaki, preparation of Nd/Na heterogeneous catalyst from bench-stable and inexpensive Nd salt for an anti-selective catalytic asymmetric nitroaldol reaction, *Tetrahedron Lett.*, 2016, **57**, 1815–1819.

78 T. Ogawa, N. Kumagai and M. Shibasaki, Self-assembling neodymium/sodium heterobimetallic asymmetric catalyst confined in a carbon nanotube network, *Angew. Chem., Int. Ed.*, 2013, **52**, 6196–6201.

79 T. Nitabaru, A. Nojiri, M. Kobayashi, N. Kumagai and M. Shibasaki, Anti-selective catalytic asymmetric nitroaldol reaction via a heterobimetallic heterogeneous catalyst, *J. Am. Chem. Soc.*, 2009, **131**, 13860–13869.

80 D. Xu, Q. Sun, Z. Quan, W. Sun and X. Wang, The synthesis of chiral tridentate ligands from L-proline and their application in the copper(II)-catalyzed enantioselective Henry reaction, *Tetrahedron: Asymmetry*, 2017, **28**, 954–963.

81 G. Lu, F. Zheng, L. Wang, Y. Guo, X. Li, X. Cao, C. Wang, H. Chi, Y. Dong and Z. Zhang, Asymmetric Henry reaction catalyzed by Cu(II)-based chiral amino alcohol complexes with C2-symmetry, *Tetrahedron: Asymmetry*, 2016, **27**, 732–739.

82 F. Xu, L. Yan, C. Lei, H. Zhao and G. Li, Asymmetric Cu-catalyzed Henry reaction promoted by chiral camphor-derived β-amino alcohols with a thiophene moiety, *Tetrahedron: Asymmetry*, 2015, **26**, 338–343.

83 F. Xu, C. Lei, L. Yan, J. Tu and G. Li, Copper–chiral camphor β–amino alcohol complex catalyzed asymmetric Henry reaction, *Chirality*, 2015, **27**, 761–765.

84 W. Jin, X. Li and B. Wan, A highly diastereo-and enantioselective copper(I)-catalyzed Henry reaction using a bis (sulfonamide)– diamine ligand, *J. Org. Chem.*, 2011, **76**, 484–491.

85 Z. L. Guo, S. Zhong, Y. B. Li and G. Lu, Chiral 1, 1′-binaphthylazepine derived amino alcohol catalyzed asymmetric Henry reaction, *Tetrahedron: Asymmetry*, 2011, **22**, 238–245.

86 D. Xin, Y. Ma and F. He, Synthesis of new planar chiral [2.2] paracyclophane Schiff base ligands and their application in the asymmetric Henry reaction, *Tetrahedron: Asymmetry*, 2010, **21**, 333–338.

87 H. Y. Kim and K. Oh, Brucine-derived amino alcohol catalyzed asymmetric Henry reaction: an orthogonal enantioselectivity approach, *Org. Lett.*, 2009, **11**, 5682–5685.

88 M. Çolak, T. Aral, H. Hoşgören and N. Demirel, Synthesis of novel chiral Schiff-base ligands and their application in asymmetric nitro aldol (Henry) reaction, *Tetrahedron: Asymmetry*, 2007, **18**, 1129–1133.

89 H. Cruz, G. Aguirre, D. Madrigal, D. Chávez and R. Somanathan, Enantioselective nitromethane addition to brominated and fluorinated benzaldehydes (Henry reaction) catalyzed by chiral bisoxazoline–copper(II) complexes, *Tetrahedron: Asymmetry*, 2016, **27**, 1217–1221.

90 L. W. Tang, X. Dong, Z. M. Zhou, Y. Q. Liu, L. Dai and M. Zhang, The first 4, 4′-imidazolium-tagged C 2-symmetric bis (oxazolines): application in the asymmetric Henry reaction, *RSC Adv.*, 2015, **5**, 4758–4765.

91 E. Wolińska, Chiral oxazoline ligands containing a 1, 2, 4-triazine ring and their application in the Cu-catalyzed asymmetric Henry reaction, *Tetrahedron*, 2013, **69**, 7269–7278.

92 K. Balaraman, R. Vasanthan and V. Kesavan, Asymmetric Henry reaction catalyzed by novel chiral bioxazolines from tartaric acid, *Synthesis*, 2012, 2455–2462.

93 W. Yang and D. Du, Highly Enantioselective Henry reaction catalyzed by C2−symmetric modular BINOL–oxazoline Schiff base copper(II) complexes generated in situ, *Eur. J. Org. Chem.*, 2011, 1552–1556.

94 K. Lang, J. Park and S. Hong, Development of bifunctional aza-bis (oxazoline) copper catalysts for enantioselective henry reaction, *J. Org. Chem.*, 2010, **75**, 6424–6435.

95 S. K. Ginotra and V. K. Singh, Enantioselective Henry reaction catalyzed by a C 2-symmetric bis (oxazoline)–Cu $(OAc)_2{\cdot}H_2O$ complex, *Org. Biomol. Chem.*, 2007, **5**, 3932.

96 F. Liu, S. Gou and L. Li, Symmetric Henry reactions of aldehydes with various nitroalkanes catalyzed by copper (II) complexes of novel chiral N–monoalkyl cyclohexane–1,2−diamines, *Appl. Organomet. Chem.*, 2014, **28**, 186–193.

97 R. Kowalczyk, Ł. Sidorowicz and J. Skarżewski, Asymmetric Henry reaction catalyzed by chiral secondary diamine-copper(II) complexes, *Tetrahedron: Asymmetry*, 2008, **19**, 2310–2315.

98 K. Mondal and S. Mistri, Schiff base based metal complexes: A review of their catalytic activity on aldol and Henry reaction, *Comments Inorg. Chem.*, 2023, **43**, 77–105.

99 M. Sharma, B. Das, G. V. Karunakar, L. Satyanarayana and K. K. Bania, Chiral Ni-Schiff base complexes inside zeolite-Y and their application in asymmetric Henry reaction: effect of initial activation with microwave irradiation, *J. Phys. Chem.*, 2016, **120**, 13563–13573.

100 G. Ouyang, Y. He and Q. Fan, Podand-based dimeric chromium(III)–salen complex for asymmetric Henry reaction: cooperative catalysis promoted by complexation of alkali metal ions, *Chem. – Eur. J.*, 2014, **20**, 16454–16457.

101 J. D. White and S. Shaw, A new catalyst for the asymmetric Henry reaction: synthesis of β-nitroethanols in high enantiomeric excess, *Org. Lett.*, 2012, **14**, 6270–6273.

102 R. Kowalczyk, P. Kwiatkowski, J. Skarżewski and J. Jurczak, Enantioselective nitroaldol reaction catalyzed by sterically modified salen−chromium complexes, *J. Org. Chem.*, 2009, **74**, 753–756.

103 J. Guo and J. Mao, Asymmetric Henry reaction catalyzed by bifunctional copper–based catalysts, *Chirality*, 2009, **21**, 619–627.

104 Y. A. Casao, E. M. Lopez and R. P. Herrera, Organocatalytic enantioselective Henry reactions, *Symmetry*, 2011, **3**, 220–245.
105 T. Marcelli, R. N. S. van der Haas, J. H. van Maarseveen and H. Hiemstra, Asymmetric organocatalytic Henry reaction, *Angew. Chem., Int. Ed.*, 2006, **45**, 929–931.
106 Aldehyde activation by H-bonding with water molecules preorganized by a Cu(II) center was suggested by Larionov, Belokon, *et al.*: V. A. Larionov, L. V. Yashkina, M. G. Mendvedev, A. F. Smol'yakov, A. S. Peregudov, A. A. Pavlov, D. B. Eremin, T. F. Savel'yeva, V. I. Maleev and Y. N. Belokon, Henry reaction revisited. Crucial role of water in an asymmetric Henry reaction catalyzed by chiral NNO-type copper(II) complexes, *Inorg. Chem.*, 2019, **58**, 11051–11065.
107 P. Clapés, W. D. Fessner, G. A. Sprenger and A. K. Samland, Recent progress in stereoselective synthesis with aldolases, *Curr. Opin. Chem. Biol.*, 2010, **14**, 154–167.
108 F. Willig, J. Lang, A. C. Hans, M. R. Ringenberg, D. Pfeffer, W. Frey and R. Peters, Polyfunctional imidazolium aryloxide betaine/Lewis acid catalysts as tools for the asymmetric synthesis of disfavored diastereomers, *J. Am. Chem. Soc.*, 2019, **141**, 12029–12043.
109 V. Miskov-Pajic, F. Willig, D. M. Wanner, W. Frey and R. Peters, Enantiodivergent [4 + 2] cycloaddition of dienolates by polyfunctional Lewis acid/zwitterion catalysis, *Angew. Chem.*, 2020, **132**, 20045–20049.
110 D. Uraguchi and T. Ooi, Chemistry of ammonium betaines: application to ion-pair catalysis for selective organic transformations, *J. Synth. Org. Chem., Jpn.*, 2018, **76**, 1144–1153.
111 X. Ye and C.-H. Tan, Enantioselective transition metal catalysis directed by chiral cations, *Chem. Sci.*, 2021, **12**, 533–539.
112 H. K. Adams, M. Kadarauch, N. J. Hodson, A. R. Lit and R. J. Phipps, Design approaches that utilize ionic interactions to control selectivity in transition metal catalysis, *Chem. Rev.*, 2025, **125**, 2846–2907.
113 A. Bürstner, P. M. Becker, A. Allgaier, L. Pfitzer, D. M. Wanner, J. Dollinger, F. Willig, J. Herrmann, V. Miskov-Pajic, A. C. Hans, W. Frey, J. van Slageren, J. Kästner and R. Peters, Tunable endo/exo selectivity in direct catalytic asymmetric 1,3−dipolar cycloadditions with polyfunctional lewis acid/azolium–aryloxide catalysts, *Angew. Chem., Int. Ed.*, 2025, **64**, e202508024.
114 D. M. Wanner, P. M. Becker, S. Suhr, N. Wannenmacher, S. Ziegler, J. Herrmann, F. Willig, J. Gabler, K. Jangid, J. Schmid, A. C. Hans, W. Frey, B. Sarkar, J. Kästner and R. Peters, Cooperative Lewis acid–1, 2, 3−triazolium–aryloxide catalysis: pyrazolone addition to nitroolefins as entry to diaminoamides, *Angew. Chem.*, 2023, **135**, e202307317.
115 Y. Zhou, J. Dong, F. Zhang and Y. Gong, Synthesis of C1-symmetric chiral secondary diamines and their applications in the asymmetric copper(II)-catalyzed Henry (nitroaldol) reactions, *J. Org. Chem.*, 2011, **76**, 588–600.
116 A. Toussaint and A. Pfaltz, Asymmetric Henry reactions catalyzed by metal complexes of chiral boron-bridged bisoxazoline (borabox) ligands, *Eur. J. Org. Chem.*, 2008, 4591–4597.
117 A. Chougnet, G. Zhang, K. Liu, D. Haussinger, A. Kagi, T. Allmendinger and W. D. Woggon, Diastereoselective and Highly Enantioselective Henry Reactions using C1-Symmetrical Copper(II) Complexes, *Adv. Synth. Catal.*, 2011, **353**, 1797–1806.
118 A. C. Hans, P. M. Becker, J. Haußmann, S. Suhr, D. M. Wanner, V. Lederer, F. Willig, W. Frey, B. Sarkar, J. Kästner and R. Peters, A Practical and robust zwitterionic cooperative lewis acid/acetate/benzimidazolium catalyst for direct 1,4-additions, *Angew. Chem., Int. Ed.*, 2023, **62**, e202217519.
119 J. Schmid, T. Junge, J. Lang, W. Frey and R. Peters, Polyfunctional bis-Lewis-acid-/bis-triazolium catalysts for stereo-selective 1,4-additions of 2-oxindoles to maleimides, *Angew. Chem., Int. Ed.*, 2019, **58**, 5447–5451.
120 M. Mechler and R. Peters, Diastereodivergent asymmetric 1,4-addition of oxindoles to nitroolefins by using polyfunctional nickel-hydrogen-bond-azolium catalysts, *Angew. Chem., Int. Ed.*, 2015, **54**, 10303–10307.
121 J. Burés, A simple graphical method to determine the order in catalyst, *Angew. Chem., Int. Ed.*, 2016, **55**, 2028–2031.
122 J. Burés, Variable time normalization analysis: general graphical elucidation of reaction orders from concentration profiles, *Angew. Chem., Int. Ed.*, 2016, **55**, 16084–16087.
123 C. D. T. Nielsen and J. Burés, Visual kinetic analysis, *Chem. Sci.*, 2019, **10**, 348–353.
124 T. Satyanarayana, S. Abraham and H. B. Kagan, Nonlinear effects in asymmetric catalysis, *Angew. Chem., Int. Ed.*, 2009, **48**, 456–494.
125 H. B. Kagan, Practical consequences of non–linear effects in asymmetric synthesis, *Adv. Synth. Catal.*, 2001, **343**, 227–233.
126 W. L. Driessen and W. L. Groeneveld, Nitromethane as a ligand. Part I: complexes with some divalent metals and the hexachloroantimonate anion, *Recl. Trav. Chim. Pays-Bas*, 1969, **88**, 491–498.
127 A. M. Wright, G. Wu and T. W. Hayton, Late-metal nitrosyl cations: synthesis and reactivity of $[Ni(NO)(MeNO_2)_3][PF_6]$, *Inorg. Chem.*, 2011, **50**, 11746–11753.
128 A. Klamt and G. Schüürmann, COSMO: a new approach to dielectric screening in solvents with explicit expressions for the screening energy and its gradient, *J. Chem. Soc., Perkin Trans. 2*, 1993, 799–805.
129 S. Grimme, S. Ehrlich and L. Goerigk, Effect of the damping function in dispersion corrected density functional theory, *J. Comput. Chem.*, 2011, **32**, 1456–1465.
130 C. Bannwarth, S. Ehlert and S. Grimme, GFN2-xTB—An accurate and broadly parametrized self-consistent tight-

binding quantum chemical method with multipole electrostatics and density-dependent dispersion contributions, *J. Chem. Theory Comput.*, 2019, **15**, 1652–1671.

131 P. Pracht, F. Bohle and S. Grimme, Automated exploration of the low-energy chemical space with fast quantum chemical methods, *Phys. Chem. Chem. Phys.*, 2020, **22**, 7169–7192.

132 F. Weigend and R. Ahlrichs, Balanced basis sets of split valence, triple zeta valence and quadruple zeta valence quality for H to Rn: Design and assessment of accuracy, *Phys. Chem. Chem. Phys.*, 2005, **7**, 3297.

133 S. Grimme, J. Antony, S. Ehrlich and H. Krieg, A consistent and accurate ab initio parametrization of density functional dispersion correction (DFT-D) for the 94 elements H-Pu, *J. Chem. Phys.*, 2010, **132**, 154104.

134 A. D. Becke, *Phys. Rev.*, 1988, **38**, 3098–3100.

135 S. Grimme, J. G. Brandenburg, C. Bannwarth and A. Hansen, Density-functional exchange-energy approximation with correct asymptotic behavior, *J. Chem. Phys.*, 2015, **143**, 3098.

136 J. Kästner, J. M. Carr, T. W. Keal, W. Thiel, A. Wander and P. Sherwood, DL-FIND: an open-source geometry optimizer for atomistic simulations, *J. Phys. Chem. A*, 2009, **113**, 11856–11865.

137 P. Sherwood, A. H. de Vries, M. F. Guest, G. Schreckenbach, C. R. A. Catlow, S. A. French, A. A. Sokol, S. T. Bromley, W. Thiel, A. J. Turner, S. Billeter, F. Terstegen, S. Thiel, J. Kendrick, S. C. Rogers, J. Casci, M. Watson, F. King, E. Karlsen, M. Sjøvoll, A. Fahmi, A. Schäfer and C. Lennartz, QUASI: A general purpose implementation of the QM/MM approach and its application to problems in catalysis, *J. Mol. Struct.: THEOCHEM*, 2003, **632**, 1–28.

138 *TURBOMOLE V7.7.1 2022*, a development of University of Karlsruhe and Forschungszentrum Karlsruhe GmbH, 1989–2007, TURBOMOLE GmbH, since 2007, available from **https://www.turbomole.org**.

139 D. Bhattacharyya, C. E. Hamrin Jr and R. P. Northey, Oxidation of hazardous organics in a two-phase fluorocarbon-water system, *Hazard. Waste Hazard. Mater.*, 1986, **3**, 405–427.

140 D. Turnbull and S. H. Maron, The ionization constants of aci and nitro forms of some nitroparaffins, *J. Am. Chem. Soc.*, 1943, **65**, 212–218.

141 M. Besora and F. Maseras, Microkinetic modeling in homogeneous catalysis, *Wiley Interdiscip. Rev.:Comput. Mol. Sci.*, 2018, **8**, e1372.

142 S. Persson, F. Fröhlich, S. Grein, T. Loman, D. Ognissanti, V. Hasselgren, J. Hasenauer and M. Cvijovic, PEtab.jl: advancing the efficiency and utility of dynamic modelling, *Bioinformatics*, 2025, **41**, btaf497.

143 T. E. Loman, Y. Ma, V. Ilin, S. Gowda, N. Korsbo, N. Yewale, C. Rackauckas and S. A. Isaacson, Catalyst: Fast and flexible modeling of reaction networks, *PLoS Comput. Biol.*, 2023, **19**, e1011530.

144 O. V. Khromova, L. V. Yashkina, N. V. Stoletova, V. I. Maleev, Y. N. Belokon and V. A. Larionov, Selectivity control in nitroaldol (Henry) reaction by changing the basic anion in a chiral copper(II) complex based on (S)-2-aminomethylpyrrolidine and 3,5-di-tert-butylsalicylaldehyde, *Molecules*, 2024, **29**, 5207.

145 M. A. Ei-Atawy, K. D. Khalil and A. H. Bashal, Chitosan capped copper oxide nanocomposite: efficient, recyclable, heterogeneous base catalyst for synthesis of nitroolefins, *Catalysts*, 2022, **12**, 964.

146 T. Jose, J. Ftouni and P. C. A. Bruijnincx, Structured hydroxyapatite composites as efficient solid base catalysts for condensation reactions, *Catal. Sci. Technol.*, 2021, **11**, 3428.